MECHANICS OF ADVANCED MATERIALS AND STRUCTURES
https://doi.org/10.1080/15376494.2023.2211069

Taylor & Francis
Taylor & Francis Group

ORIGINAL ARTICLE

Molecular dynamics simulation of free transverse vibration behavior of single-walled coiled carbon nanotubes

Farshid Darvishi[a], Omid Rahmani[a], Alireza Ostadrahimi[b], Eunsoo Choi[c], and Guoqiang Li[b]

[a]Smart Structures and Advanced Materials Laboratory, Department of Mechanical Engineering, University of Zanjan, Zanjan, Iran; [b]Department of Mechanical and Industrial Engineering, Louisiana State University, Baton Rouge, LA, USA; [c]Department of Civil Engineering, Hongik University, Seoul, South Korea

ABSTRACT

Coiled carbon nanotubes (CCNTs) belong to one of the prominent classes of carbon nanostructures with unique mechanical properties and vibrational behavior due to their helical geometries. In this paper, the free transverse vibration behavior of single-walled CCNTs is investigated by molecular dynamics (MD) simulations and the adaptive intermolecular reactive empirical bond-order (AIREBO) potential under different boundary conditions (B.Cs.). The beating phenomenon is observed in CCNTs due to the presence of longitudinal, transverse, and torsional coupled vibrations and the proximity of their corresponding frequency. Generally, the frequency of the CCNTs decreases by increasing the length (L) or the number of pitches (n_p). Moreover, the pitch angle ($\overline{\alpha}$) plays a more decisive role compared to other geometric parameters. At constant length (L) of CCNTs, the frequency increases by enhancing the pitch angle ($\overline{\alpha}$). Furthermore, the fundamental frequency range of the studied CCNTs is obtained less than 331.9 GHz for lengths greater than 2 nm under different boundary conditions. This indicates that CCNTs have a higher vibration sensitivity than straight CNTs. Therefore, CCNTs can be a proper alternative to straight CNTs in sensors. The results of this study can be used in the design and analysis of nanoelectromechanical systems (NEMs) with CCNTs elements as well as to calibrate continuum mechanics methods.

ARTICLE HISTORY
Received 15 January 2023
Accepted 3 May 2023

KEYWORDS
Beating phenomenon; coiled carbon nanotubes (CCNTs); molecular dynamics (MD) simulations; transverse vibration

1. Introduction

Carbon nanotubes (CNTs) are discovered by Ijima in 1991 and have several applications in different materials [1–6]. Different arrangements of non-hexagonal rings, such as the pentagons and heptagons, in the hexagonal network of CNTs, create positive and negative curvatures that can bend and twist CNTs to form other morphologies, such as coiled carbon nanotubes (CCNTs) [7].

Catalytic chemical vapor deposition (CCVD) is a common technique for the synthesis of CCNTs. Xie et al. [8] used thermal filament and microwave CCVD techniques to prepare CCNTs. Figure 1 represents the images taken from the CCNTs' morphology using the scanning electron microscope (SEM) and the transmission electron microscope (TEM).

CCNTs have shown potential applications in various fields due to their unique spiral structures and extraordinary physical characteristics. An essential application of CCNTs is to operate as sensors. CCNTs with attached electrodes can be used as self-sensing mechanical resonators to detect the fundamental resonances ranging from 100 to 400 MHz. The self-sensing CCNTs sensors are sensitive to mass change and well suited for measuring small forces and masses in the femtogram range [9]. Moreover, CCNTs can be applied as high-resolution force sensors in conjunction with visual displacement measurement as well as electromechanical sensors [10]. Another application of CCNTs involves their usage in reinforced high-strain composites due to their higher toughness compared to the carbon fibers. In comparison with CNTs, they can be better anchored in their embedding matrix [11]. Some other applications of CCNTs include their application in nano-electromechanical systems (NEMS) [12] such as nano-spring, nano-actuators, nano-gears, and nano-receivers as well as nonvolatile random access memory (NVRAM) [13]. Furthermore, they could be employed in nano-switches and electromagnetic nano-transformers as molecular nano-solenoids [14]. The mechanical properties and vibrational behavior of CCNTs should be well understood to establish a better paradigm of their applications. Theoretical methods are preferred since experimental studies at nanoscale size are quite expensive and time-consuming. Atomic-scale methods such as molecular dynamics (MD) simulation can be useful in the study of nanostructures [15–20]. Nguyen et al. [15] investigated through molecular dynamics finite element method with Tersoff potential the buckling behavior of boron nitride (BN) nanotubes under bending. Shima et al. [19] performed molecular dynamics simulations of multi-walled carbon nanotubes under hydrostatic pressure to elucidate the novel class of radial buckling in the systems. Ansari et al. [20] studied the effects of initial

CONTACT Alireza Ostadrahimi aostad3@lsu.edu Department of Mechanical and Industrial Engineering, Louisiana State University, Baton Rouge, LA 70803, USA.

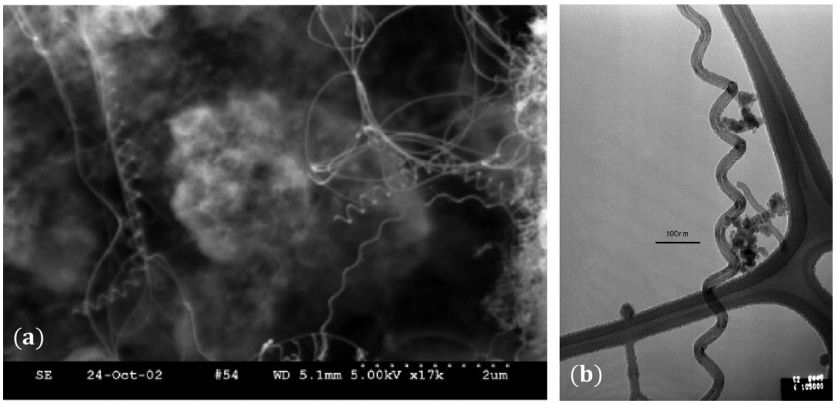

Figure 1. Images of CCNTs that synthesized using CCVD technique. (a) SEM, (b) TEM [8].

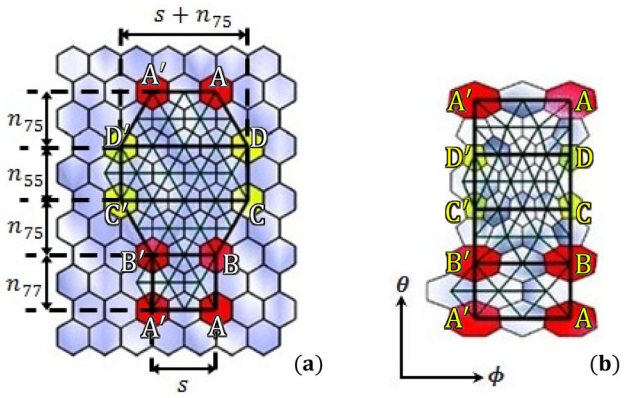

Figure 2. (a) Primary unit cell, (b) New unit cell (parametric rectangular plane) mapped from primary unit cell.

thermal loading on the vibrational behavior of embedded single-walled carbon nanotubes (SWCNTs) based on the nonlocal shell model and examined the accuracy of their model by comparison with molecular dynamics simulation results.

Furthermore, several theoretical studies were carried out to assess the mechanical properties of single-walled CCNTs and CCNT-reinforced nanocomposites. Fonseca et al. [21] used the Kirchhoff rod model to derive a series of expressions for determining Young's modulus and Poisson's ratio of CCNTs. Liu et al. [22] employed the density functional theory (DFT) and tight-binding (TB) to assess the Young's modulus and elastic constant of a set of CCNTs built from the armchair single-walled CNTs and predicted their superelastic behavior. Ghaderi and Hajiesmaili [23] used an MD-based finite element method to determine fracture strain, fracture load, and energy storage density of the CCNTs. Wang et al. [24] applied the MD simulations and the second generation of the reactive empirical bond order (REBO) potential and Lennard–Jones (LJ) potential to evaluate the mechanical properties of a CCNT under compression, tension, re-compression, re-tension, and pullout from a polyethylene (PE) matrix. They obtained spring constants, yielding strains, and pullout force of the CCNT. Wu et al. [25] used the MD simulations and the adaptive intermolecular reactive empirical bond-order (AIREBO) potential to study the stretching instability and reversibility of tightly wound CCNTs and determine their stiffness and gravimetric toughness. Sharifian et al. [26] investigated the role of chemical doping in the large deformation behavior of the CCNTs via the MD simulations and the AIREBO potential. They identified mechanical properties such as tensile strength, ultimate failure strain, and toughness during the tensile test stages for various ranges of geometries and chemical doping percentages. Khani et al. [27], Kianfar et al. [28], and Yarali et al. [29] adopted a new representative volume element (RVE) algorithm to study the elastic properties of CCNTs-reinforced polymer nanocomposites and the thermomechanical properties of CCNTs-reinforced shape memory polymer nanocomposites. In these studies, the effect of volume fraction, orientation, and geometrical parameters of CCNTs were also examined on the elastic and thermomechanical properties.

So far, the free vibration behavior of CCNTs has been investigated in several theoretical studies [30–34]. Fakhrabadi et al. [30], examined the vibrational behavior of the single-walled CCNTs using molecular mechanics (MM) based finite element method and 3-D elastic beam elements. They determined the natural frequencies and mode shapes of CCNTs with different geometries and in various boundary conditions. Darvishi and Rahmani [32] investigated the free longitudinal vibration of single-walled CCNTs via the MD simulations with aid of the REBO potential. They evaluated the influence of different parameters, including the diameter of tubes, number of pitches, and various boundary conditions on the fundamental frequencies. Mohammadi and Farid [33] analyzed free vibration of helically coiled carbon nanotubes considering nonlocal effects using a spatial curved-beam model. They used finite element method to solve the resulting equations, numerically. The results obtained from the proposed method by neglecting nonlocal effects were compared with those of ANSYS simulation. Besides, the effects of different boundary conditions and various parameters including the helix radius, pitch, number of turns, and nonlocal parameter on the natural frequencies were studied. Darvishi and Rahmani [34] investigated the size-dependent vibration behavior of doubly clamped single-walled coiled carbon nanotubes (CCNTs) via nonlocal helical beam model. Their model was based on Washizu's beam model and taking into account transverse shear deformations. They solved the nonlocal governing equations, by the generalized differential quadrature method (GDQM). Then, the natural frequencies and corresponding mode shapes were determined for the

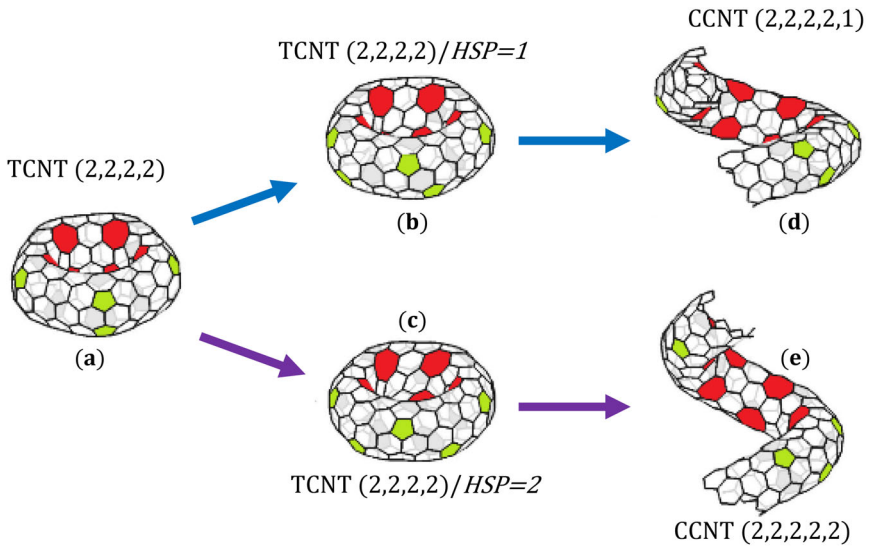

Figure 3. (a) D_{5h}-symmetric TCNT with indices $(2,2,2,2)$, (b) TCNT$(2,2,2,2)$ with $HSP = 1$, (c) TCNT$(2,2,2,2)$ with $HSP = 2$, (d) CCNT(2,2,2,2,1) made of TCNT$(2,2,2,2)$ with $HSP = 1$, (e) CCNT(2,2,2,2,2) made of TCNT$(2,2,2,2)$ with $HSP = 2$.

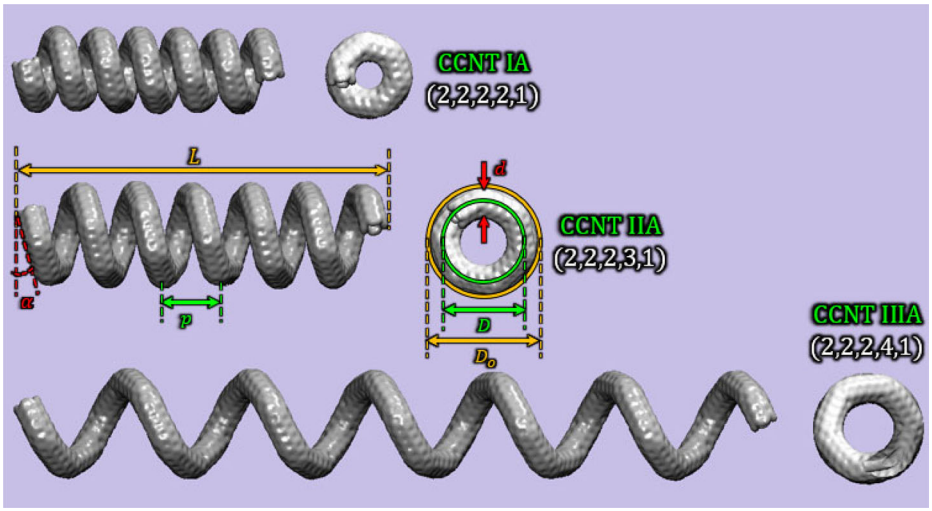

Figure 4. Image of six pitches of CCNTs—A.

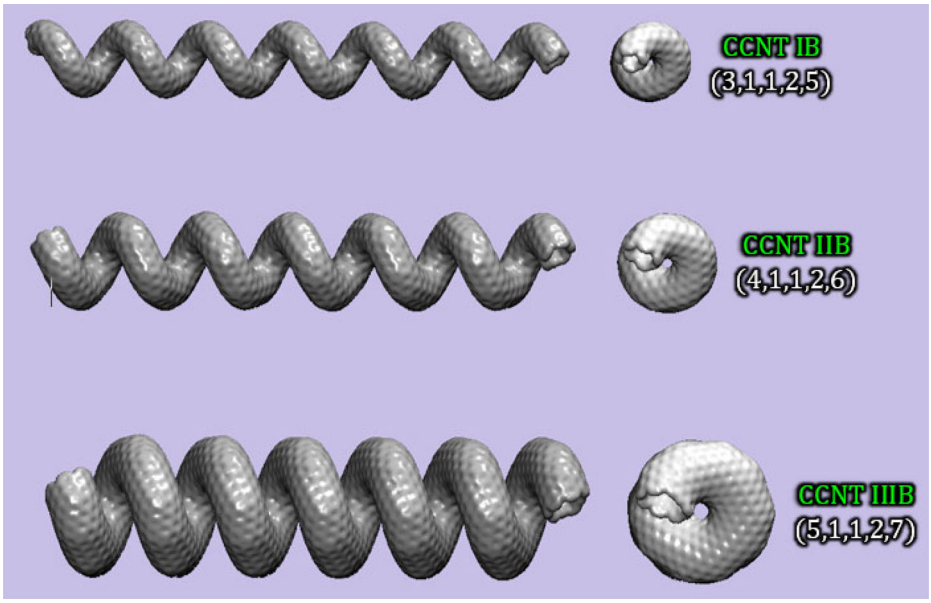

Figure 5. Image of six pitches of CCNTs—B.

Table 1. Geometric characteristics of CCNT samples.

CCNTs−A	CCNT IA $(2,2,2,2,1)$ ▷ $d=0.546$ nm; $D=1.474$ nm; $p=1.032$ nm; $\bar{\alpha}=12.57°$							
	L	2.226	3.368	4.348	5.327	6.306	7.449	8.428
	n_p	2.157	3.264	4.213	5.162	6.111	7.218	8.167
	N_a	648	984	1272	1560	1848	2184	2472
	CCNT IIA $(2,2,2,3,1)$ ▷ $d=0.546$ nm; $D=1.974$ nm; $p=1.448$ nm; $\bar{\alpha}=13.14°$							
	LoC	3.174	4.542	5.909	7.503	8.815	10.238	11.834
	n_p	2.192	3.137	4.081	5.182	6.088	7.071	8.173
	N_a	872	1256	1640	2088	2472	2856	3304
	CCNT IIIA $(2,2,2,4,1)$ ▷ $d=0.546$ nm; $D=2.072$ nm; $p=3.112$ nm; $\bar{\alpha}=25.55°$							
	L	6.202	9.420	12.271	15.482	18.697	21.915	25.129
	n_p	1.993	3.027	3.943	4.975	6.008	7.042	8.075
	N_a	968	1448	1864	2344	2824	3304	3784
CCNTs−B	CCNT IB $(3,1,1,2,5)$ ▷ $d=0.584$ nm; $D=0.998$ nm; $p=1.888$ nm; $\bar{\alpha}=31.04°$							
	L	3.455		5.128	7.220	9.291		11.402
	n_p	1.830		2.716	3.824	4.921		6.039
	N_a	538		762	1042	1322		1602
	CCNT IIB $(4,1,1,2,6)$ ▷ $d=0.757$ nm; $D=1.244$ nm; $p=1.890$ nm; $\bar{\alpha}=25.81°$							
	L	3.530		5.553	7.577	9.599		11.217
	n_p	1.868		2.938	4.009	5.079		5.935
	N_a	678		1162	1562	1962		2282
	CCNT IIIB $(5,1,1,2,7)$ ▷ $d=0.989$ nm; $D=1.525$ nm; $p=1.734$ nm; $\bar{\alpha}=19.90°$							
	L	3.392		5.171	6.952	8.731		10.511
	n_p	1.956		2.982	4.009	5.035		6.062
	N_a	1438		2138	2838	3538		4238

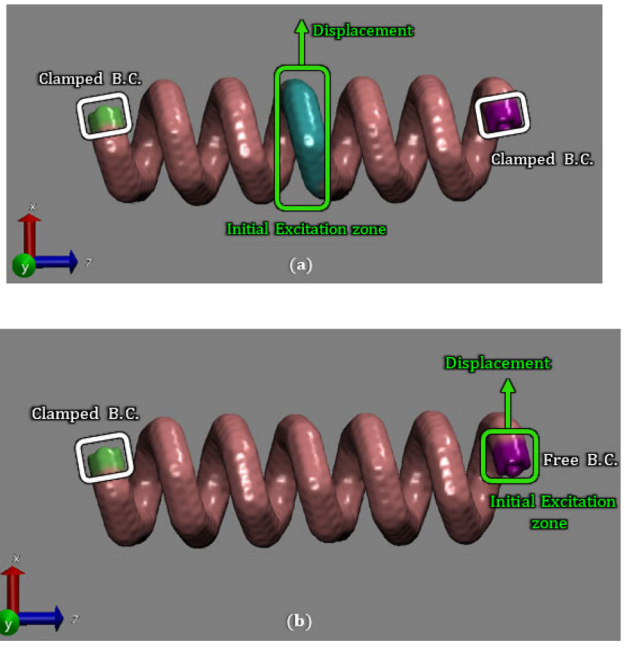

Figure 6. Applying the boundary conditions and displacement to establish the initial excitation of CCNTs. (a) C−C boundary conditions (b) C−F boundary conditions.

clamped-clamped boundary conditions. After that, a parametric study on the effect of different parameters, including the helix cylinder to tube diameters ratio (D/d), number of pitches, helix pitch angle, and nonlocal parameter on the natural frequencies of CCNTs was conducted. As can be seen from the literature review, studies in the field of the vibrational behavior of CCNTs are very limited, necessitating further research to broaden our insight into the vibrational behavior of the CCNTs.

The main purpose of this paper is thus the investigation of the free transverse vibration behavior of the CCNTs. First, CCNTs are modeled and their fundamental transverse frequencies are determined by MD simulations based on AIREBO potential. The complex and unique geometric form of these nanostructures and the simultaneous occurrence of tensile, flexural, and torsional deformations led to vibrational coupling, which is examined in detail in the present study. Moreover, the effects of geometrical parameters of CCNTs as well as boundary conditions are evaluated on the fundamental transverse frequencies.

2. Methodology

2.1. Modeling of the CCNTs

In this research, CCNTs are modeled using the dual space topological approach proposed in [35, 36]. According to Figure 2a, a balloon-shaped cut is first made in the perfect graphene sheet which is considered as a unit cell in terms of four parametric indices $(n_{75}, n_{77}, n_{55}, s)$. n_{75} is the vertical topological distance between adjacent heptagons (red-rings) and pentagons (green-rings), n_{77} represents the topological distance between adjacent heptagons, n_{55} shows the topological distance between adjacent pentagons, and s denote the length of the unit cell. This unit cell is then meshed into equilateral triangles (called dual space) such that the atoms inside the unit cell are at the center of these triangles. Then, the atoms inside the unit cell are mapped to a new unit cell, called a parametric rectangular plane, in terms of coordinates (θ,ϕ) as shown in Figure 2b. Note that heptagons (red-rings) and pentagons (green-rings) are Stone-Wales defects, thus, the presence of these carbon rings is necessary for the formation of TCNTs and CCNTs.

TCNT is modeled by repeating n of the new unit cells in the ϕ direction followed by its rolling in the θ direction, and then geometrical optimization (Figure 3a). Two types of symmetry can be considered for TCNTs: D_{nh}-symmetric TCNT resembling hollow-prism, and D_{nd}-symmetric TCNT, which is similar to hollow-antiprism.

According to Figure 3b and 3c, a distortion process, called the horizontal shifting process (*HSP*), is carried out to create CCNTs. In general, the *HSP* operation leads to

Table 2. Minimization process of the CCNT IIA for optimization of the structure.

CCNT IIA (2,2,2,3,1)						
Number of pitches	Minimization stats					
	Initial energy (eV)	Final energy (eV)	Cohesive energy E_c^* (eV)	Initial pressure (bar)	Final pressure (bar)	Iterations
2.192	−6181.54	−6246.71	7.1637	−176.43344	−0.00036	1627
3.137	−8919.44	−9012.20	7.1753	−316.22761	−0.00043	2652
4.081	−11657.34	−11777.70	7.1815	−289.94351	−0.00011	3516
5.182	−14851.56	−15004.10	7.1859	−439.45249	−0.00020	4957
6.088	−17589.46	−17769.60	7.1883	−483.51109	−0.00006	6018
7.071	−20327.36	−20535.09	7.1902	−521.70451	0.00065	6922
8.173	−23521.58	−23761.50	7.1917	−560.41004	0.00014	9699
9.117	−26259.48	−26526.99	7.1928	−589.43324	0.00001	10910

*Cohesive energy E_c(eV) ≈ Final energy per atom (eV/atom)

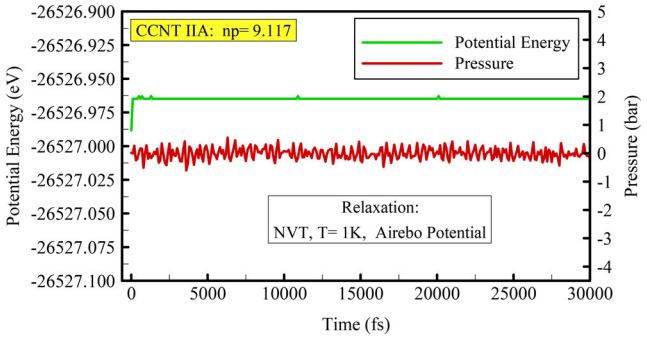

Figure 7. Variations of the potential energy and pressure of the CCNT IIA with $n_p = 9.117$ in the relaxation process (the temperature was controlled at 1K by Nose–Hoover thermostat).

considerable strain and consequently high structural unstability in the TCNT. The distorted TCNT can release its additional strain by cutting out the bonds on a certain longitude and recoils to form a CCNT. The pitch angle of CCNT in $HSP = 2$ is larger than $HSP = 1$ because of the larger distortion and strain energy (Figure 3d and 3e) [35]. From now on, CCNTs can be expressed with five parametric indices $(n_{75}, n_{77}, n_{55}, s, HSP)$.

In the present study, two classes of D_{nh}-symmetric CCNTs are modeled: CCNTs−A and CCNTs−B. According to Figures 4 and 5, the CCNTs−A includes three samples CCNT IA (2,2,2,2,1), CCNT IIA(2,2,2,3,1), and CCNT IIIA(2,2,2,4,1) whereas the CCNTs−B encompassed three samples of CCNT IB(3,1,1,2,5), CCNT IIB(4,1,1,2,6), and CCNT IIIB(5,1,1,2,7). The geometric characteristics, number of pitches (n_p) and number of atoms (N_a) of these CCNTs are listed in Table 1. In which d, D, D_o, p, $\overline{\alpha}$, and L are diameter, coil median diameter, coil outer diameter, pitch length, pitch angle, and lenght of the CCNTs, respectively. It should be noted that $D_o = D + d$ and $L = n_p p$.

2.2. Molecular dynamics simulation

In the present study, the large-scale atomic/molecular massively parallel simulator (LAMMPS) package software [37] is utilized for MD simulations of free vibration behavior of the CCNTs. Interatomic interactions of the CCNTs is modeled with the aid of the AIREBO potential which can be expressed by the following equation:

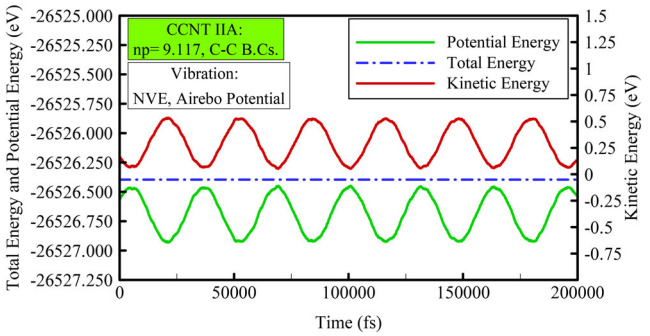

Figure 8. Variation of the potential energy, kinetic energy, and total energy of the CCNT IIA with $n_p = 9.117$ in the free vibration process under C−C boundary conditions.

$$U^{AIREBO} = \frac{1}{2}\sum_{i}\sum_{i\neq j}\left[U_{ij}^{REBO} + U_{ij}^{LJ} + \sum_{k\neq i,j}\sum_{l\neq i,j,k} U_{kijl}^{Torsion}\right] \quad (1)$$

The AIREBO potential includes three types of potentials: the REBO potential for bonded interatomic interactions, the LJ potential for nonbonded interatomic interactions, and dihedral torsion potential for torsional interatomic interactions. The LJ potential in AIREBO potential considers long-range interactions greater than 2°A up to the maximum cutoff radius $r_{c-\max}$ (i.e. $2°\text{A} \leq r_{c-LJ} \leq r_{c-\max}$). The maximum cutoff radius of the LJ potential is often considered $r_{c-\max} = 10.2°\text{A}$ [25]. Excessively large selection of the cutoff radius for LJ potential, leads to excessive stiffness and consequently higher frequencies in CCNTs, which can be undesirable. The shrink-wrapped (s) type non-periodic boundary conditions (NPBCs) are considered for the walls of the simulation box in all three directions of x, y, and z. The time step of the simulation is 1 femtosecond (fs) and the unit of measure is Metal. The simulation steps involve the following stages:

1. *Minimization*: After modeling the CCNTs, the energy minimization process is performed by the conjugate gradient (CG) method to optimize the geometry of these nanostructures. By iterative adjustment of the coordinates of the atoms and satisfying one of the stopping criteria, the configuration of the structure reaches the local potential energy minimum.
2. *Relaxation*: At this stage, the initial velocity of the atoms is first allocated based on the Maxwell–Boltzmann distribution [38] at temperature of 1 K. Newtonian equations of motion are then numerically integrated using the Velocity–Verlet algorithm [39] to update the positions and velocities of the atoms. The relaxation process is performed by the canonical (NVT) ensemble at 1 K so that the temperature is controlled through the Nose–Hoover thermostat [40]. At the end of this process, the CCNTs reach an equilibrium state. It is worth noting that in the MD simulation of free vibration of straight CNTs, the temperature value was taken into account as 1 K to prevent the effect of the temperature on the natural frequencies and coupling of transverse and longitudinal vibrations [41]. Forasmuch as the coupling of transverse, longitudinal, and torsional

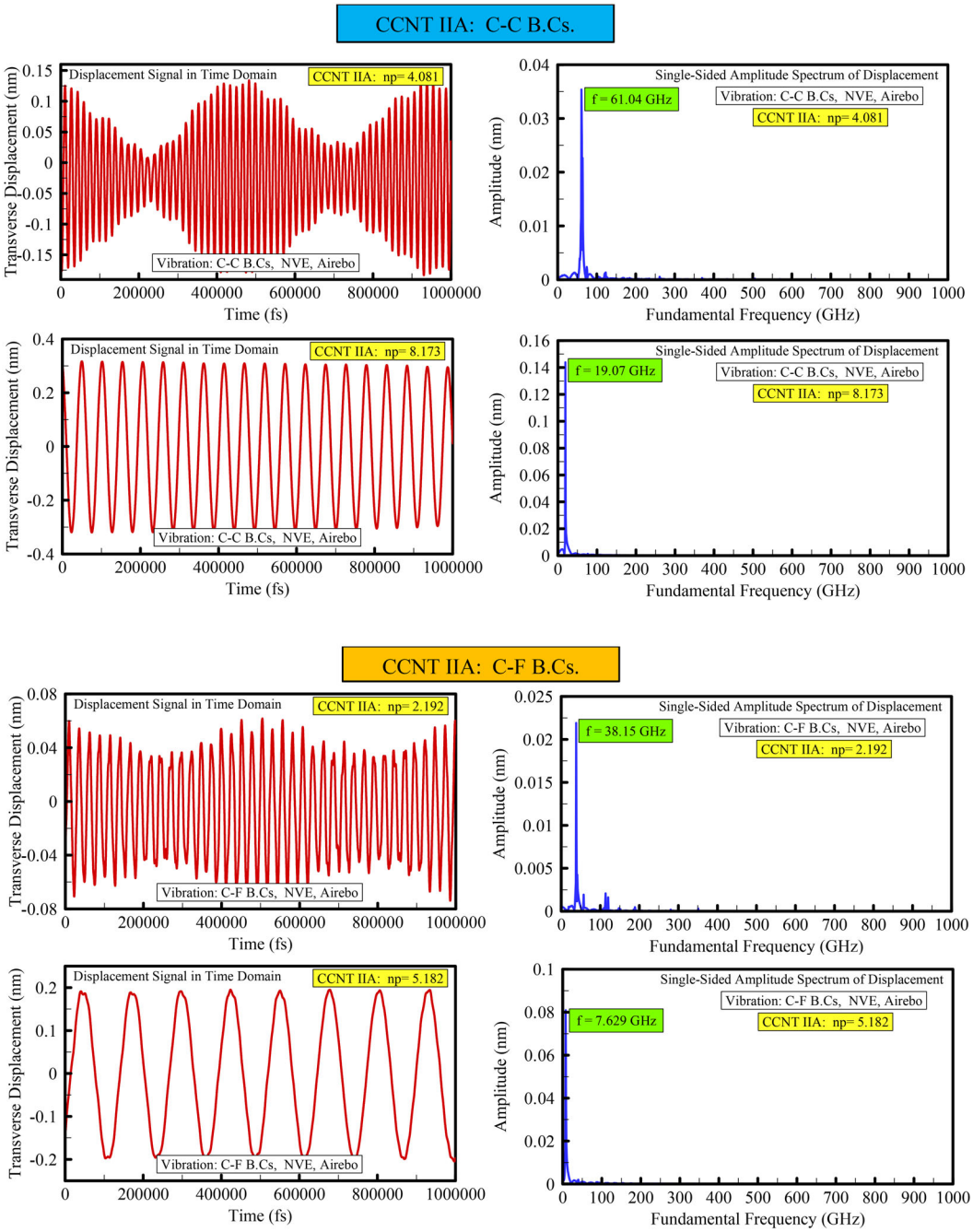

Figure 9. Transverse displacement–time diagrams (left) and frequency domain signal diagrams (right) of CCNT IIA with different number of pitches under C−C and C−F boundary conditions.

vibrations is significantly evident in the CCNTs, by choosing a temperature of 1 K, the vibrations coupling tried to be prevented as much as possible.

3. *Applying the boundary conditions and initial excitation*: In this study, the initial excitation technique is used to analyze the free transverse vibration of CCNTs. This technique is one of the most widely used techniques for experimental evaluation of the frequency response of the structure [42]. After the relaxation process of CCNTs at 1 K, the canonical (NVT) ensemble is canceled and the initial excitation process of CCNTs is carried out to determine free vibration in the microcanonical (NVE) ensemble under clamped-clamped (C−C) and clamped-free (C−F) boundary conditions. For the C−C boundary conditions as shown in Figure 6a, two regions with four atomic layers on the left (green region) and right (purple region) of CCNTs are entirely fixed in all three directions. Whereas for the C−F boundary conditions (Figure 6b), only one region with four atomic layers on the left (green region) of CCNTs is fully fixed in all three directions.

The initial excitation must be appropriately applied to the desired vibrating mode with the predetermined mode shape. For the first mode shape, the initial excitation zones in the C−C and C−F boundary conditions are at the middle and end of the CCNT, respectively

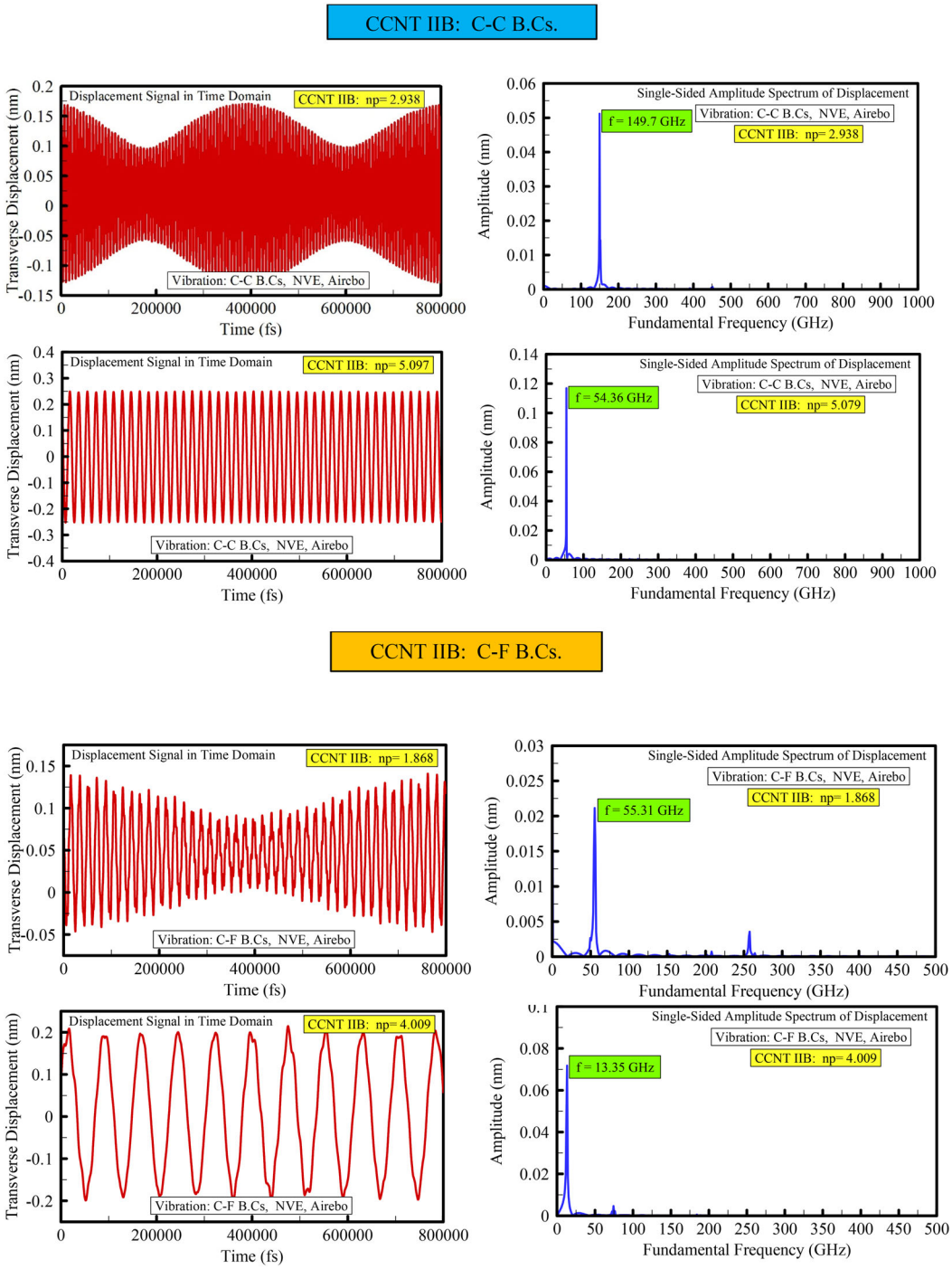

Figure 10. Transverse displacement-time diagrams (left) and frequency domain signal diagrams (right) of CCNT IIB with different number of pitches under C−C and C−F boundary conditions.

(zones marked with green frameworks in Figure 6). The initial excitation amplitude W is considered to be 5% of the CCNTs length, namely:

$$W = 5\% \times L \tag{2}$$

4. *Free Vibration*: After applying a displacement with amplitude W to atoms of the excitation zone, they are released so that CCNTs begin to vibrate freely. To ignore the effect of initial excitation, free vibration analysis is performed after 30,000 fs. A time range of 500,000 to 2,500,000 fs is considered to establish the free vibration process depending on the length of CCNTs and boundary conditions. Within this time range, the transverse displacement-time history of the center of mass of the atoms of the CCNTs is recorded in each timestep as a time-domain response. Next, the time domain signals of the transverse displacement are converted into a frequency domain signals using the fast Fourier transform (FFT) method in MATLAB software.

3. Results and discussions

Table 2 presents the status of the CCNT IIA minimization for different number of pitches. The structure of the

Table 3. Fundamental transverse frequencies of CCNTs−A obtained from MD simulation under C−C and C−F boundary conditions.

Fundamental transverse frequency (GHz)								
CCNT IA	B.Cs.	Lenght of CCNTs (nm)							
		2.226	3.368	4.348	5.327	6.306	7.449	8.428	9.408
	C−C	213.6	145.9	101.1	74.39	56.27	43.87	34.33	28.61
	C−F	67.71	34.33	21.93	15.26	10.49	7.629	5.722	4.768
CCNT IIA	B.Cs.	Lenght of CCNTs (nm)							
		3.174	4.542	5.909	7.503	8.815	10.238	11.834	13.201
	C−C	130.7	88.69	61.04	41.96	32.42	24.80	19.07	16.21
	C−F	38.15	20.98	12.40	7.629	5.722	3.815	3.338	2.861
CCNT IIIA	B.Cs.	Lenght of CCNTs (nm)							
		6.202	9.420	12.271	15.482	18.697	21.915	25.129	28.347
	C−C	92.51	54.36	35.29	22.89	16.21	12.40	9.537	7.629
	C−F	20.98	9.537	5.722	3.815	2.384	1.907	1.431	1.192

CCNT IA $\triangleright$ $d = 0.546$nm; $D = 1.474$nm; $D_o = 2.020$nm; $p = 1.032$nm; $\bar{\alpha} = 12.57^\circ$
CCNT IIA $\triangleright$ $d = 0.546$nm; $D = 1.974$nm; $D_o = 2.520$nm; $p = 1.448$nm; $\bar{\alpha} = 13.14^\circ$
CCNT IIIA $\triangleright$ $d = 0.546$nm; $D = 2.072$nm; $D_o = 2.618$nm; $p = 3.112$nm; $\bar{\alpha} = 25.55^\circ$

Table 4. Fundamental transverse frequencies of CCNTs−B obtained from MD simulation under C−C and C−F boundary conditions.

Fundamental transverse frequency (GHz)						
CCNT IB	B.Cs.	Lenght of CCNTs (nm)				
		3.455	5.128	7.220	9.291	11.402
	C−C	331.9	185.0	100.1	62.94	42.92
	C−F	59.13	28.61	15.26	9.537	6.199
CCNT IIB	B.Cs.	Lenght of CCNTs (nm)				
		3.530	5.553	7.577	9.599	11.217
	C−C	312.8	149.7	84.88	54.36	41.01
	C−F	55.31	23.84	13.35	8.106	5.993
CCNT IIIB	B.Cs.	Lenght of CCNTs (nm)				
		3.392	5.171	6.952	8.731	10.511
	C−C	206.9	112.5	67.71	44.82	32.42
	C−F	40.05	19.07	10.49	7.153	4.768

CCNT IB $\triangleright$ $d = 0.584$nm; $D = 0.998$nm; $D_o = 1.582$nm; $p = 1.888$nm; $\bar{\alpha} = 31.04^\circ$
CCNT IIB $\triangleright$ $d = 0.757$nm; $D = 1.244$nm; $D_o = 2.001$nm; $p = 1.890$nm; $\bar{\alpha} = 25.81^\circ$
CCNT IIIB $\triangleright$ $d = 0.989$nm; $D = 1.525$nm; $D_o = 2.514$nm; $p = 1.734$nm; $\bar{\alpha} = 19.90^\circ$

CCNT reaches its energy minima and residual pressure or stress is eliminated with energy-based stopping tolerance of $etol = 10^{-30}$ and force-based stopping tolerance of $ftol = 10^{-30}\text{eV}/^\circ\text{A}$.

The average cohesive energy (energy per unit atom) for the CCNT IIA, at end of the minimization, is obtained as 7.184 eV. Milosevic et al. [43] determined the cohesive energy for a group of CCNTs via density functional tight binding (DFTB) method in the range of 7.46–8.00 eV. This implies that the results of the present study are in good agreement with them. The energy level of the CCNT decreases by elevating the number of pitches and atoms.

The relaxation process for $n_p = 9.117$ of the CCNT IIA is presented in Figure 7. The potential energy and pressure fluctuate around a constant value over a time of 30,000 fs. This state indicates the equilibrium conditions and stability of the CCNTs.

In the following, the variations of the potential energy, kinetic energy, and total mechanical energy for $n_p = 9.117$ of the CCNT IIA are presented in Figure 8 during the free vibration under C−C boundary conditions. As can be seen, the total mechanical energy of the CCNTs remains constant due to the adiabatic conditions of the system in the micro-canonical (NVE) ensemble

Figures 9 and 10, respectively, illustrate how to determine the values of fundamental transverse frequencies of CCNT IIA and CCNT IIB with different lengths (or number of pitches) under C−C and C−F boundary conditions. The transverse displacement-time domain signal diagrams are also depicted on the left side while the frequency domain signal diagrams determined from fast Fourier transform (FFT) are demonstrated on the right side. The first peak in the frequency domain signal diagram represents the fundamental transverse frequency (first mode).

As shown in the transverse displacement–time diagrams, after applying the initial transverse excitation to CCNTs along the x-direction (Figure 6), the vibration amplitude increases and decreases continuously over time, and CCNTs displays a behavior similar to the beating phenomenon. Since there is no excitation force in free vibration to induce the beating phenomenon, the origin of this phenomenon can be explained as follows:

The vibrational coupling (longitudinal along the z-direction, transverse along the x, y-directions, and torsion along the s-direction) occurs in CCNTs due to the co-occurrence of tensile, bending, and torsional deformations. In other words, the vibrations of CCNTs can simultaneously occur in three directions. As we know, the beating phenomenon

Table 5. Fundamental transverse frequencies of CCNTs obtained from MM-based finite element method by Fakhrabadi et al. [30] under C−C and C−F boundary conditions.

		Fundamental transverse frequency (GHz)								
CCNT *a*	B.Cs.	Lenght of CCNTs (nm)								
		2.990	4.485	5.980	7.475	8.970	10.465	11.960	13.455	14.950
	C−C	306.88	171.15	115.08	79.672	59.016	39.379	29.508	23.606	17.705
	C−F	86.029	41.912	24.265	15.441	13.235	8.823	6.618	4.412	2.206
CCNT *b*	B.Cs.	Lenght of CCNTs (nm)								
		4.090	6.135	8.180	10.225	12.270	14.315	16.360	18.405	20.450
	C−C	369.00	168.60	101.79	76.346	50.897	31.811	25.449	19.086	12.724
	C−F	77.080	33.034	17.618	11.011	6.607	4.404	2.202	0.971	0.485
CCNT *c*	B.Cs.	Lenght of CCNTs (nm)								
		3.680	5.520	7.360	9.200	11.040	12.880	14.720	16.560	18.400
	C−C	617.65	277.94	150.98	96.078	65.196	41.176	27.451	24.020	20.588
	C−F	92.232	35.323	19.624	15.699	9.812	7.849	5.887	3.925	1.962

CCNT $a \triangleright$ $d = 0.734$nm; $D = 1.224$nm; $D_o = 1.958$nm; $p = 1.495$nm; $\bar{\alpha} = 21.24°$
CCNT $b \triangleright$ $d = 0.786$nm; $D = 0.916$nm; $D_o = 1.702$nm; $p = 2.045$nm; $\bar{\alpha} = 35.40°$
CCNT $c \triangleright$ $d = 0.877$nm; $D = 1.188$nm; $D_o = 2.065$nm; $p = 1.840$nm; $\bar{\alpha} = 26.24°$

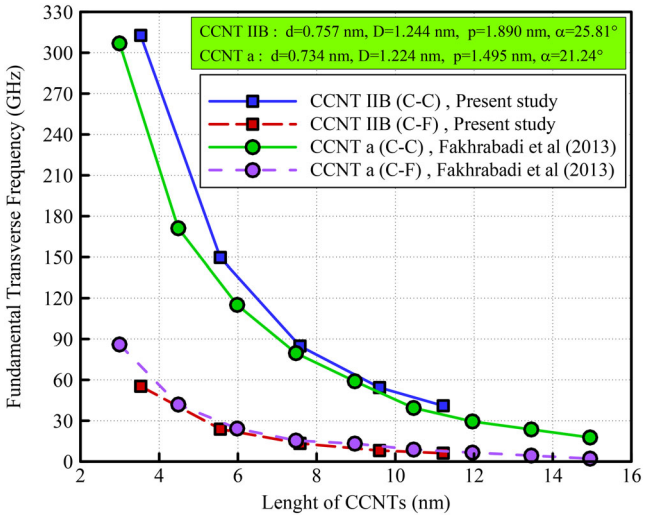

Figure 11. A comparison between the results of CCNT IIB in the present study with the results of CCNT *a* obtained by Fakhrabadi et al. [30] for almost identical geometric parameters.

occurs when the excitation frequency is close to the natural frequencies (not exactly equal to it). Let f_n shows the frequency corresponding to a given transverse free vibration (for example, along the x-direction) and f_n' represent the frequency corresponding to vibrations along other directions. In that case, CCNTs face specific situations in which the beating phenomenon are expected to occur because of proximity of the frequencies values f_n' to the transverse frequency values f_n.

Also, the beating phenomenon occurs earlier for lower length (or the number of pitches) due to intense coupling between transverse, longitudinal, and torsional vibrations, as well as the proximity of their frequencies to each other. Moreover, as shown in the frequency signal diagrams, the first peak emerges earlier when the length (or the number of pitches) is increased, indicating an inverse relationship between frequency and length.

The results of free vibration of the CCNTs−A and CCNTs−B are reported in Tables 3 and 4 for different lengths under C−C and C−F boundary conditions.

The findings of Fakhrabadi et al. [30] on the free vibration of the three samples CCNTs (namely: CCNT *a*, CCNT *b*, and CCNT *c*) are reported in Table 5. They investigated the vibrational modal analysis of the CCNTs using a molecular mechanics (MM)-based finite element method, in which bonds were considered as elastic beam elements whose constants were determined by the force field.

To validate the present study, the results of CCNT IIB are compared with the results of CCNT *a* (Figure 11). These two CCNTs have almost identical diameters (d) and coil median diameters (D). It can be seen that the results of the present method are in good agreement with the method of Fakhrabadi et al. [30]. The slight difference in the results can be due to the difference in the computational method and values of the pitch angle ($\bar{\alpha}$) these two CCNTs.

As can be seen from Tables 4 and 5, the fundamental transverse frequency of the CCNTs decreases as the length (or the number of pitches) increases. Moreover, the type of boundary conditions significantly affects the vibration frequencies of CCNTs. The C−C boundary conditions always result in higher frequencies than C − F boundary conditions. In the C − C boundary conditions, the stiffness of the CCNTs increases by reducing the degrees of freedom (DoF) of the structure, leading to higher frequencies.

In the CCNTs−A, which have the same diameter (d), the fundamental frequency increases by elevating the coil median diameter (D) and the pitch angle ($\bar{\alpha}$) for the same length (L) under both C−C and C−F boundary conditions.

In the CCNTs−B, however, the rise the diameter (d) and coil median diameter (D) and a decline in the pitch angle ($\bar{\alpha}$) decrements the fundamental frequency decreases for the same length (L) under both boundary conditions. On the other hand, Fakhrabadi et al. [30] did not report a specific trend for the frequency of CCNTs versus the geometric parameters. In general, it can be said that the pitch angle ($\bar{\alpha}$) has a more decisive role on the vibrational behavior of CCNTs than other geometric parameters, and the frequency values are directly related to it.

Table 6. Fundamental transverse frequencies of straight CNTs obtained from MD simulation under C−C and C−F boundary conditions [39,40].

Fundamental transverse frequency (GHz)								
Ansari et al. [44]	CNT (5,5)	B.Cs.	Lenght of CNTs (nm)					
			2.428	3.671	4.897	6.123	7.349	8.592	9.818
		C−C	1977.7	954.1	554.4	343.8	199.3	123.3	52.04
		C−F	435.6	208.9	119.0	69.40	52.22	34.37	27.10
	CNT (10,10)	B.Cs.	Lenght of CNTs (nm)						
			2.428	3.671	4.897	6.123	7.349	8.592	9.818
		C−C	2242.3	1164.4	771.8	547.0	407.2	307.6	234.0
		C−F	667.6	343.0	193.0	126.2	89.23	67.42	48.25
Hu et al. [40]	CNT (5,5)	B.Cs.	Lenght of CNTs (nm)						
			1.698	2.912	4.124	5.333	8.974		
		C−C	–	1065.5	659.3	–	179.3		
		C−F	560.3	231.7	137.1	80.40	33.09		
	CNT (10,10)	B.Cs.	Lenght of CNTs (nm)						
			1.698	2.912	4.124	5.333	8.974		
		C−C	–	1200.8	816.1	–	283.3		
		C−F	778.5	391.4	228.0	141.9	55.91		
	CNT (15,15)	B.Cs.	Lenght of CNTs (nm)						
			1.698	2.912	4.124	5.333	8.974		
		C−F	849.2	458.9	295.4	189.9	73.85		
	CNT (20,20)	B.Cs.	Lenght of CNTs (nm)						
			1.698	2.912	4.124	5.333	8.974		
		C−F	865.0	485.3	319.8	–	94.94		

CNT $(5,5) \triangleright D_o = 0.678$nm ; CNT $(10,10) \triangleright D_o = 1.357$nm
CNT $(15,15) \triangleright D_o = 2.035$nm ; CNT $(20,20) \triangleright D_o = 2.714$nm

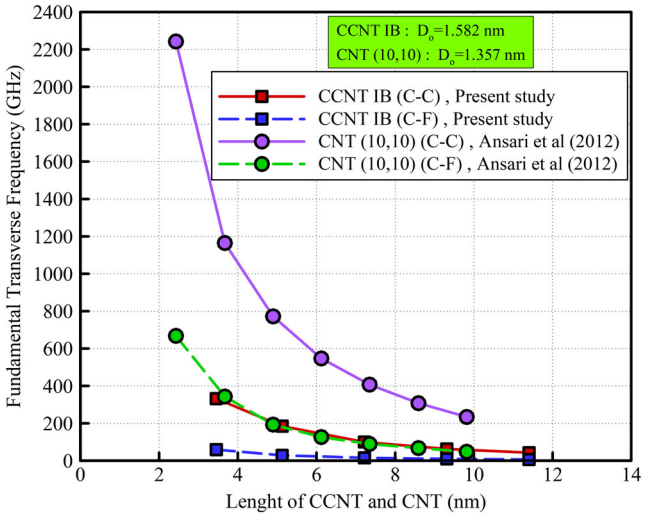

Figure 12. A comparison between the results of CCNT IB in the present study with the results of CNT (10,10) obtained by Ansari et al. [44] for the same length (L) and outer diameter (D_o).

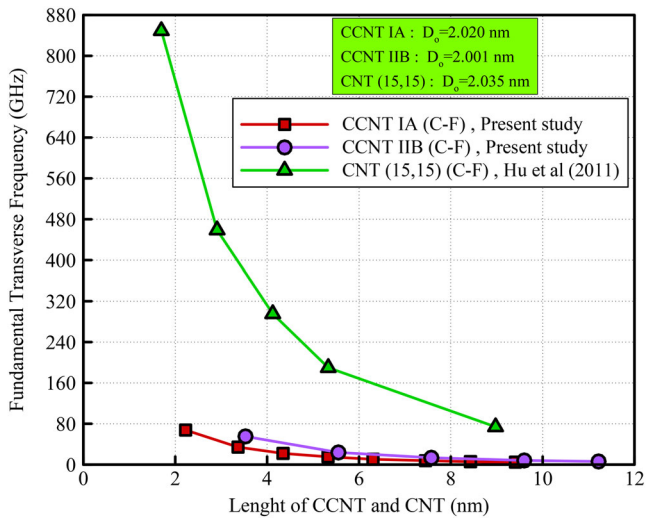

Figure 13. A comparison between the results of CCNT IA and CCNT IIB in the present study with the results of CNT (15,15) obtained by Hu et al. [45] for the same length (L) and outer diameter (D_o).

In the following, the free vibration behavior of CCNTs is compared with the straight CNTs. The fundamental transverse frequencies of straight CNTs are reported in Table 6. These results were obtained by Ansari et al. [44] and Hu et al. [45] using molecular dynamics (MD) simulations. In straight CNTs, the frequencies increases by enlarging the outer diameter (D_o) for the same length (L). The frequency values are always greater in C−C boundary conditions as compared with C−F boundary conditions. To compare the fundamental transverse frequencies, CCNTs and CNTs are considered with similar outer diameters (D_o) and lengths (L). The CCNT IB and CNT (10,10) have approximately the same outer diameter (i.e. $D_o = 1.582$nm and $D_o = 1.357$nm, respectively).

Also, the CCNT IA, CCNT IIB, and CNT (15,15) have the same outer diameter (i.e. $D_o = 2.202$nm, $D_o = 2.001$nm, and $D_o = 2.035$nm, respectively). As shown in Figures 12 and 13, the fundamental transverse frequencies of the straight CNTs are considerably larger than the CCNTs for the same outer diameter (D_o) and length (L). It means that CCNTs have lower stiffness than straight CNTs for the same diameter and length. Furthermore, it can be said that CCNTs have a higher vibration sensitivity than straight CNTs.

4. Conclusions

In this paper, the free transverse vibration behavior of CCNTs was studied using the molecular dynamics (MD)

simulations. For this purpose, first, two classes of the CCNTs with different geometric characteristics were modeled, then the interatomic interactions were described in them using the AIREBO potential. After the energy minimization and relaxation processes, CCNTs vibrated by applying initial transverse excitation under clamped-clamped (C−C) and clamped-Free (C−F) boundary conditions. Finally, the fundamental transverse frequencies of the CCNTs were determined for different lengths (or number of pitches) using the fast Fourier transform (FFT) of the time domain signal to the frequency domain signal. The results revealed that:

- The beating phenomenon occurred in the CCNTs due to the vibration coupling (longitudinal along the z-direction, transverse along the x, y-directions, and torsion along the s -direction). This phenomenon took place earlier for shorter lengths (or fewer number of pitches).
- In general, as the length (or the number of pitches) of the CCNTs increased, the fundamental transverse frequency decremented.
- The pitch angle ($\overline{\alpha}$) played a more decisive role on the vibrational behavior of CCNTs compared to other geometric parameters, and frequency values were directly related to it.
- In the case of CCNTs, the C−C boundary conditions always result in higher frequencies compared to the C−F boundary conditions.
- The results indicated the higher vibration sensitivity of CCNTs compared to straight CNTs. Thus, CCNTs can be a proper alternative to straight CNTs in sensing applications.

Acknowledgments

This work was supported by a grant from the National Research Foundation of Korea (NRF) funded by the Korean government (MEST) (Project No. NRF 2019R1A2C-2008542).

Disclosure statement

The authors declare that they have no known competing financial interests or personal relationships that could have appeared to influence the work reported in this paper.

Data and code availability

Not applicable.

Supplementary information

Not applicable.

Ethical approval

Not applicable.

ORCID

Alireza Ostadrahimi http://orcid.org/0000-0002-1179-4833
Eunsoo Choi http://orcid.org/0000-0001-9687-8288
Guoqiang Li http://orcid.org/0000-0002-7004-6659

References

[1] S. Iijima, Helical microtubules of graphitic carbon, Nature, vol. 354, no. 6348, pp. 56–58, 1991. DOI: 10.1038/354056a0.
[2] N. Jain, E. Gupta, and N.J. Kanu, Plethora of carbon nanotubes applications in various fields—A state-of-the-art-review, Smart Sci., vol. 10, no. 1, pp. 1–24, 2022. (published online) DOI: 10.1080/23080477.2021.1940752.
[3] E. Choi, A. Ostadrahimi, and H. Youn, Analytical and experimental study of shape memory alloy reinforcement on the performance of butt-fusion welded joints in high-density polyethylene pipe, J. Intell. Mater. Syst. Struct., vol. 31, no. 17, pp. 2029–2043, 2020. DOI: 10.1177/1045389X20942583.
[4] S. Sarrafan and G. Li, A hybrid syntactic foam-based open-cell foam with reversible actuation, ACS Appl. Mater. Interfaces, vol. 14, no. 45, pp. 51404–51419, 2022. DOI: 10.1021/acsami.2c16168.
[5] R. Wang, L. Sun, X. Zhu, W. Ge, H. Li, Z. Li, H. Zhang, Y. Huang, Z. Li, Y.-F. Zhang, J. Zhao, Q. Xu, and H. Lan, Carbon nanotube-based strain sensors: Structures, Adv. Mater. Technol., vol. 8, no. 1, pp. 2200855, 2023. DOI: 10.1002/admt.202200855.
[6] E. Choi, A. Ostadrahimi, J.H. Lee, and L.S. Jeon, On the efficiency of induced prestressing in SMA mortar beams through different thermal stimuli, Smart Mater. Struct., vol. 31, no. 12, pp. 125026, 2022. DOI: 10.1088/1361-665X/aca3e2.
[7] L. Liu, F. Liu, and J. Zhao, Curved carbon nanotubes: From unique geometries to novel properties and peculiar applications, Nano Res., vol. 7, no. 5, pp. 626–657, 2014. DOI: 10.1007/s12274-014-0431-1.
[8] J. Xie, K. Mukhopadyay, J. Yadev, and V. Varadan, Catalytic chemical vapor deposition synthesis and electron microscopy observation of coiled carbon nanotubes, Smart Mater. Struct., vol. 12, no. 5, pp. 744–748, 2003. DOI: 10.1088/0964-1726/12/5/010.
[9] A. Volodin, D. Buntinx, M. Ahlskog, A. Fonseca, J.B. Nagy, and C. Van Haesendonck, Coiled carbon nanotubes as self-sensing mechanical resonators, Nano Lett., vol. 4, no. 9, pp. 1775–1779, 2004. DOI: 10.1021/nl0491576.
[10] D.J. Bell, Y. Sun, L. Zhang, L.X. Dong, B.J. Nelson, and D. Grutzmacher, Three-dimensional nanosprings for electromechanical sensors. In: The 13th International Conference on Solid-State Sensors, Actuators and Microsystems, pp. 15–18. Vol. 11, 2005.
[11] K. Hernadi, L. Thiên-Nga, and L. Forró, Growth and microstructure of catalytically produced coiled carbon nanotubes, J. Phys. Chem. B., vol. 105, no. 50, pp. 12464–12468, 2001. DOI: 10.1021/jp011208p.
[12] K.T. Lau, M. Lu, and D. Hui, Coiled carbon nanotubes: Synthesis and their potential applications in advanced composite structures, Compos. B: Eng., vol. 37, no. 6, pp. 437–448, 2006. DOI: 10.1016/j.compositesb.2006.02.008.
[13] J.H. Chang and W. Park, Nano elastic memory using carbon nanocoils, J. Nano Bio Technol., vol. 3, no. 1, pp. 30–35, 2006.
[14] K. Akagi, R. Tamura, M. Tsukada, S. Itoh, and S. Ihara, Electronic structure of helically coiled cage of graphitic carbon, Phys. Rev. Lett., vol. 74, no. 12, pp. 2307–2310, 1995. DOI: 10.1103/PhysRevLett.74.2307.
[15] V.-T. Nguyen, D.-T. Nguyen, and M.-Q. Le, Bending of boron nitride nanotubes: An atomistic study, Mech. Adv. Mater. Struct., vol. 26, no. 16, pp. 1357–1364, 2019. DOI: 10.1080/15376494.2018.1432801.
[16] R. Izadi, M. Tuna, P. Trovalusci, and N. Fantuzzi, Bending characteristics of carbon nanotubes: Micropolar elasticity

models and molecular dynamics simulations, Mech. Adv. Mater. Struct., vol. 30, no. 1, pp. 189–206, 2023. DOI: 10.1080/15376494.2021.2011499.

[17] S. Nakarmi and V.U. Unnikrishnan, Understanding size and strain induced variabilities in thermal conductivity of carbon nanotubes: A molecular dynamics study, Mech. Adv. Mater. Struct., vol. 29, no. 14, pp. 1977–1985, 2022. DOI: 10.1080/15376494.2020.1846232.

[18] N. Chandra and S. Namilae, Tensile and compressive behavior of carbon nanotubes: Effect of functionalization and topological defects, Mech. Adv. Mater. Struct., vol. 13, no. 2, pp. 115–127, 2006. DOI: 10.1080/15376490500343816.

[19] H. Shima, Y. Umeno, and M. Sato, Molecular dynamics study of radial corrugation in carbon nanotubes, Mech. Adv. Mater. Struct., vol. 22, no. 6, pp. 423–427, 2015. DOI: 10.1080/15376494.2012.761303.

[20] R. Ansari, J. Torabi, and M. Faghih Shojaei, An efficient numerical method for analyzing the thermal effects on the vibration of embedded single-walled carbon nanotubes based on the nonlocal shell model, Mech. Adv. Mater. Struct., vol. 25, no. 6, pp. 500–511, 2018. DOI: 10.1080/15376494.2017.1285457.

[21] A.F. da Fonseca and D.S. Galvão, Mechanical properties of nanosprings, Phys. Rev. Lett., vol. 92, no. 17, pp. 175502, 2004. DOI: 10.1103/PhysRevLett.92.175502.

[22] L. Liu, H. Gao, J. Zhao, and J. Lu, Superelasticity of carbon nanocoils from atomistic quantum simulations, Nanoscale Res. Lett., vol. 5, no. 3, pp. 478–483, 2010. DOI: 10.1007/s11671-010-9545-x.

[23] S.H. Ghaderi and E. Hajiesmaili, Nonlinear analysis of coiled carbon nanotubes using the molecular dynamics finite element method, Mater. Sci. Eng.: A, vol. 582, pp. 225–234, 2013. DOI: 10.1016/j.msea.2013.05.060.

[24] J. Wang, T. Kemper, T. Liang, and S.B. Sinnott, Predicted mechanical properties of a coiled carbon nanotube, Carbon, vol. 50, no. 3, pp. 968–976, 2012. DOI: 10.1016/j.carbon.2011.09.060.

[25] J. Wu, J. He, G.M. Odegard, S. Nagao, Q. Zheng, and Z. Zhang, Giant stretchability and reversibility of tightly wound helical carbon nanotubes, J. Am. Chem. Soc., vol. 135, no. 37, pp. 13775–13785, 2013. DOI: 10.1021/ja404330q.

[26] A. Sharifian, V. Fadaei Naeini, M. Baniassadi, J. Wu, and M. Baghani, Role of chemical doping in large deformation behavior of spiral carbon-based nanostructures: Unraveling geometry-dependent chemical doping effects, J. Phys. Chem. C., vol. 123, no. 31, pp. 19208–19219, 2019. DOI: 10.1021/acs.jpcc.9b04894.

[27] N. Khani, M. Yildiz, and B. Koc, Elastic properties of coiled carbon nanotube reinforced nanocomposite: A finite element study, Mater. Des., vol. 109, pp. 123–132, 2016. DOI: 10.1016/j.matdes.2016.06.126.

[28] A. Kianfar, M.M. Seyyed Fakhrabadi, and M.M. Mashhadi, Prediction of mechanical and thermal properties of polymer nanocomposites reinforced by coiled carbon nanotubes for possible application as impact absorbent, Proc. Inst. Mech. Eng. C: J Mech. Eng. Sci., vol. 234, no. 4, pp. 882–902, 2020. DOI: 10.1177/0954406219885969.

[29] E. Yarali, M. Baniassadi, and M. Baghani, Numerical homogenization of coiled carbon nanotube reinforced shape memory polymer nanocomposites, Smart Mater. Struct., vol. 28, no. 3, pp. 035026, 2019. DOI: 10.1088/1361-665X/ab02b6.

[30] M.M.S. Fakhrabadi, A. Amini, F. Reshadi, N. Khani, and A. Rastgoo, Investigation of buckling and vibration properties of hetero-junctioned and coiled carbon nanotubes, Comput. Mater. Sci., vol. 73, pp. 93–112, 2013. DOI: 10.1016/j.commatsci.2013.02.020.

[31] F. Darvishi and O. Rahmani, Calibration of nonlocal generalized helical beam model for free vibration analysis of coiled carbon nanotubes via molecular dynamics simulations, Mech. Adv. Mater. Struct., vol. 30, no. 8, pp. 1624–1648, 2023. DOI: 10.1080/15376494.2022.2038739.

[32] F. Darvishi and O. Rahmani, Investigation of the free longitudinal vibration of single-walled coiled carbon nanotubes (SWCCNTs) using molecular dynamics simulation, Amirkabir J. Mech. Eng., vol. 51, no. 3, pp. 91–100, 2019.

[33] S.Z. Mohammadi and M. Farid, Free vibration analysis of helically coiled carbon nanotubes considering nonlocal effect using curved beam elements, Int. J. Multi. Comp. Eng., vol. 17, no. 1, pp. 83–97, 2019. DOI: 10.1615/IntJMultCompEng.2019015907.

[34] F. Darvishi and O. Rahmani, On the free vibration of doubly clamped single-walled coiled carbon nanotubes: A novel size dependent continuum model, J. Solid Mech., vol. 13, no. 2, pp. 114–133, 2021.

[35] C. Chuang, Y.-C. Fan, and B.-Y. Jin, Generalized classification scheme of toroidal and helical carbon nanotubes, J. Chem. Inform. Model., vol. 49, no. 2, pp. 361–368, 2009. DOI: 10.1021/ci800395r.

[36] C. Chuang, Y.-C. Fan, and B.-Y. Jin, Dual space approach to the classification of toroidal carbon nanotubes, J. Chem. Inform. Model., vol. 49, no. 7, pp. 1679–1686, 2009. DOI: 10.1021/ci900124z.

[37] S. Plimpton, A. Thompson, and P. Crozier, *Lammps molecular dynamics simulator*. Accessed http://lammps.sandia.gov/.

[38] H.J.W. Müller-Kirsten, Basics of Statistical Physics, World Scientific, Germany, 2012.

[39] H. Rafii-Tabar, Modelling the nano-scale phenomena in condensed matter physics via computer-based numerical simulations, Phys. Rep., vol. 325, no. 6, pp. 239–310, 2000. DOI: 10.1016/S0370-1573(99)00087-3.

[40] W.G. Hoover, Canonical dynamics: Equilibrium phase-space distributions, Phys. Rev. A: Gen. Phys., vol. 31, no. 3, pp. 1695–1697, 1985. DOI: 10.1103/physreva.31.1695.

[41] Y.Y. Zhang, C.M. Wang, and V.B.C. Tan, Assessment of Timoshenko beam models for vibrational behavior of single-walled carbon nanotubes using molecular dynamics, Adv. Appl. Math. Mech., vol. 1, no. 1, pp. 89–106, 2009.

[42] I.L. Chang and C.M. Huang, Vibrational behavior of single-walled carbon nanotubes: Atomistic simulations, Jpn. J. Appl. Phys., vol. 52, no. 10R, pp. 105101, 2013. DOI: 10.7567/JJAP.52.105101.

[43] I. Milošević, Z.P. Popović, and M. Damnjanović, Structure and stability of coiled carbon nanotubes, Phys. Status Solidi B., vol. 249, no. 12, pp. 2442–2445, 2012. DOI: 10.1002/pssb.201200048.

[44] R. Ansari, S. Ajori, and B. Arash, Vibrations of single- and double-walled carbon nanotubes with layerwise boundary conditions: A molecular dynamics study, Curr. Appl. Phys., vol. 12, no. 3, pp. 707–711, 2012. DOI: 10.1016/j.cap.2011.10.007.

[45] Y.-G. Hu, K.M. Liew, and Q. Wang, Nonlocal continuum model and molecular dynamics for free vibration of single-walled carbon nanotubes, J. Nanosci. Nanotechnol., vol. 11, no. 12, pp. 10401–10407, 2011. DOI: 10.1166/jnn.2011.5729.